



HAL
open science

Mechanisms of grapevine resilience to a vascular disease: investigating stem radial growth, xylem development, and physiological acclimation

Ninon Dell'Acqua, Gregory A Gambetta, Sylvain Delzon, Nathalie Ferrer,
Laurent J Lamarque, Nicolas Saurin, Pauline Theodore, Chloe E. L. Delmas

► To cite this version:

Ninon Dell'Acqua, Gregory A Gambetta, Sylvain Delzon, Nathalie Ferrer, Laurent J Lamarque, et al.. Mechanisms of grapevine resilience to a vascular disease: investigating stem radial growth, xylem development, and physiological acclimation. *Annals of Botany*, 2024, 133 (2), pp.mcad188. 10.1093/aob/mcad188 . hal-04342012

HAL Id: hal-04342012

<https://hal.inrae.fr/hal-04342012>

Submitted on 13 Dec 2023

HAL is a multi-disciplinary open access archive for the deposit and dissemination of scientific research documents, whether they are published or not. The documents may come from teaching and research institutions in France or abroad, or from public or private research centers.

L'archive ouverte pluridisciplinaire **HAL**, est destinée au dépôt et à la diffusion de documents scientifiques de niveau recherche, publiés ou non, émanant des établissements d'enseignement et de recherche français ou étrangers, des laboratoires publics ou privés.



Distributed under a Creative Commons Attribution - NonCommercial - NoDerivatives 4.0
International License

Mechanisms of grapevine resilience to a vascular disease: investigating stem radial growth, xylem development, and physiological acclimation

Ninon DELL'ACQUA¹, Gregory A. GAMBETTA², Sylvain DELZON³, Nathalie FERRER¹, Laurent J. LAMARQUE^{3,4}, Nicolas SAURIN⁵, Pauline THEODORE¹, Chloé E. L. DELMAS^{1,*}

¹INRAE, Bordeaux Sciences Agro, ISVV, SAVE, F-33140, Villenave d'Ornon, France;

²EGFV, Bordeaux-Sciences Agro, INRAE, Université de Bordeaux, ISVV, 210 chemin de Leysotte, 33882 Villenave d'Ornon, France; ³Univ. Bordeaux, INRAE, BIOGECO, 33615 Pessac, France; ⁴Département des Sciences de l'Environnement, Université du Québec à Trois-Rivières, CA; ⁵UE Pech Rouge, Univ Montpellier, INRAE, Gruissan, France

*For correspondence: chloe.delmas@inrae.fr

ABSTRACT

Background and Aims

Plant vascular diseases significantly impact crop yield worldwide. Esca is a grapevine vascular disease found globally in vineyards which causes a loss of hydraulic conductance due to the occlusion of xylem vessels by tyloses. However, the integrated response of plant radial growth and physiology in maintaining xylem integrity in grapevine expressing esca symptoms remains poorly understood.

Methods

We investigated the interplay between variation in stem diameter, xylem anatomy, plant physiological response, and hydraulic traits in two widespread esca susceptible cultivars, ‘Sauvignon blanc’ and ‘Cabernet Sauvignon’. We used an original experimental design using naturally infected mature vines which were uprooted and transplanted into pots allowing for their study in a mini-lysimeter greenhouse phenotyping platform.

Key Results

Esca significantly altered the timing and sequence of stem growth periods in both cultivars, particularly the shrinkage phase following radial expansion. Symptomatic plants had a significantly higher density of occluded vessels and lower leaf- and whole-plant gas exchange. Esca-symptomatic vines showed compensation mechanisms, producing numerous small functional xylem vessels later in development suggesting a maintenance of stem vascular cambium activity. Stabilization or late recovery of whole plant stomatal conductance coincided with new healthy shoots at the top of the plant after esca symptoms plateaued.

Conclusions

Modified cropping practices, like avoiding late season topping, may enhance resilience in esca-symptomatic plants. These results highlight that integrating dendrometers, xylem anatomy, and gas exchange provides insights into vascular pathogenesis and its effects on plant physiology.

KEYWORDS

Dendrometer, Esca, Gas exchange, Grapevine, Plant hydraulics, Radial growth, Vascular disease, Xylem anatomy

Accepted Manuscript

INTRODUCTION

The xylem tissue plays a central role in transporting water and nutrients from the roots to the leaves. This transport occurs in a metastable state under tension (Dixon and Joly 1894), and is essential for gas exchange, photosynthesis, and thus the growth and productivity of vascular plants. Disrupting the flow of water and nutrients can lead to a decrease in productivity, and if severe, to the death of the plant by hydraulic failure. Negative impacts on the plant hydraulic system can be induced by both abiotic and biotic stresses through a variety of processes (Mensah *et al.*, 2020; McDowell *et al.*, 2022). However, the impact of biotic stresses on plant hydraulics and the subsequent consequences on plant growth and mortality risk is still an incipient field of study.

Under optimal growth conditions, the long-term radial growth of plants is typically characterized by a rapid growth phase that begins in spring after winter dormancy, followed by a gradual decrease as the growing season progresses (Deslauriers *et al.*, 2007; Gruber *et al.*, 2018). However, some species such as *Vitis vinifera* deviate from this pattern by undergoing a phase of stem size reduction following the initial rapid growth phase. This shrinkage occurs at the same time as the onset of fruit ripening, and was previously thought to be due to assimilate relocation from the stem to the berries (Intrigliolo and Castel 2007). However, Van de Wal *et al.* (2018) suggest that stem shrinkage may occur due to the formation of a new periderm layer, followed by dehydration and death of tissues located beyond the newly formed periderm. Although it is widely acknowledged that biotic stresses and dieback processes have an impact on plant growth (e.g. Hartmann and Messier 2008; Oliva *et al.*, 2016; Rizzoli *et al.*, 2022), little is known regarding the real-time effects of pest and pathogen infections on stem diameter variations during these specific growth periods (see Cailleret *et al.*, 2017, Cohen *et al.*, 1997, Luque *et al.*, 1999). For example, continuous

monitoring of plant growth using stem or trunk radial dendrometers would allow the effects of biotic stresses to be linked to changes in growth, which could be integrated with gas exchange, hydraulics, and anatomy. Multi-trait approaches are crucial to improve our understanding of short-term changes in plant-pathogen interactions.

Vascular diseases occur worldwide and are caused by destructive plant pathogens (bacterial, fungal, or oomycete microorganisms) with dramatic negative impacts on crops (Yadeta and J. Thomma 2013). Vascular pathogenesis can cause hydraulic failure through the production of gums or gels (amorphous extracellular materials, Rioux *et al.*, 1998), and/or tyloses. Tyloses are vascular parenchyma invaginations within xylem vessels (Pearce 1996). These vessel occlusions presumably support compartmentalization after injury and limit the spread of wood decay organisms and pathogens, especially vascular pathogens (De Micco *et al.*, 2016). However, different vascular host-pathogen interactions have shown that vessel occlusions such as tyloses can alter water transport, decreasing hydraulic conductivity (Collins *et al.*, 2009; Urban and Dvořák 2014; Mensah *et al.*, 2020; Bortolami *et al.*, 2021a). These occlusions may be associated with a decrease in stomatal conductance (Bortolami *et al.*, 2021b; Fanton *et al.*, 2022) or not (Mensah *et al.*, 2020) likely depending on the specific plant-pathogen interaction. Recently, X-ray microtomography visualization of xylem vessels in esca symptomatic grapevines revealed hydraulic failure due to the presence of tylose and/or gel in the lumen of leaf vessels, at distance from the pathogen location in the trunk (Bortolami *et al.*, 2019). Different organs appear to be differentially impacted by these vascular occlusions. The highest level of hydraulic failure was found in the peripheral veins of esca symptomatic leaf blades with a 79 % loss of functional xylem tissue on average, as estimated using the optical vulnerability technique (Bortolami *et al.*, 2023). Using *in vivo* X-ray microtomography visualizations, the loss of hydraulic conductance measured in the midrib was 69% on average, 55% in the petiole, and 27.5% in the symptomatic current year

shoot (Bortolami *et al.*, 2019; Bortolami *et al.*, 2021a). At the same time stomatal conductance and CO₂ assimilation are reduced in symptomatic leaves (Bortolami *et al.*, 2021b). In addition, some studies have shown that pathogens have the potential to impact the cambial activity and alter xylem development in grapevine (e.g. during Eutypiosis, Rudelle *et al.*, 2005 and Flavescence dorée, Jelmini *et al.*, 2021). We can hypothesize that reduced photosynthesis along with impaired water transport due to tylosis formation during esca pathogenesis could alter radial growth and cambial activity in symptomatic stems. A better understanding of the distribution of occluded vessels within the xylem of healthy and symptomatic shoots could help identify their role in pathogenesis and their impact on plant growth and water relations.

The aim of this study was to examine the impact of the vascular disease esca on stem growth dynamics, xylem anatomy, and physiology in two susceptible widespread grapevine cultivars, ‘Sauvignon blanc’ and ‘Cabernet Sauvignon’. More specifically, we developed a multi-trait and integrative approach to monitor vascular pathogenesis and assess the putative resilience capacity of esca symptomatic plants. Esca is a grapevine vascular disease with significant negative economic impacts on viticulture (Hofstetter *et al.*, 2012; Bruez *et al.*, 2013). Although esca has been recognized for more than a hundred years (Mugnai *et al.*, 1999), it is still poorly understood, mainly because it is not yet possible to reliably reproduce the development of leaf symptoms by pathogen inoculation in the laboratory. To study esca pathogenesis under controlled conditions, we used an original experimental design made of naturally infected 20 year-old plants uprooted from two vineyards in France and transplanted into pots. Multiple traits were monitored during three months in the greenhouse: plant-water relations at the leaf and whole-plant scales (measuring whole-plant and leaf gas exchange, predawn and midday water potentials), continuous stem radial growth (using dendrometer

measurements), xylem anatomy and tylosis formation (through optical microscopy of stem and midrib cross sections), and esca leaf symptom expression.

MATERIALS AND METHODS

Plant material

Twenty year-old plants of two *Vitis vinifera* cultivars were uprooted in winter 2021 from two Bordeaux vineyards: Nine plants of ‘Sauvignon blanc’ grafted on Fercal from Couhins (44°45'17.9"N 0°33'32.6"W) and 10 plants of ‘Cabernet Sauvignon’ grafted on 101-14MGt from Luchey-Halde (44°49'25.4"N 0°37'51.4"W). Leaf symptoms have been monitored on each plant since 2012. All selected vines had expressed esca leaf symptoms at least once since 2012. We considered plants that didn't express symptoms in 2021 as controls, as we previously demonstrated that the history of leaf symptom expression in the past had no significant impact on plant physiological and hydraulic traits (Bortolami *et al.*, 2021b).

We uprooted the vines in March of 2021 and transferred them into 20L pots following the protocol detailed in (Bortolami *et al.*, 2019). Outside of the field environment, transplanting vines is the only method allowing for the study of natural esca symptom development on mature plants. Before the beginning of the experimentation, inflorescences were removed to homogenize the plant material, and during the experimentation secondary shoots were removed just after budbreak, except for the most apical secondary shoot after pruning. In the greenhouse, plants were irrigated with nutrient solution (0.1 mM NH₄H₂PO₄, 0.187 mM NH₄NO₃, 0.255 mM KNO₃, 0.025 mM MgSO₄, 0.002 mM Fe, and oligo-elements [B, Zn, Mn, Cu, and Mo]). Environmental conditions were monitored every 15 minutes using temperature and humidity probes (S-THB-M002, Onset) and global radiation sensors (S-LIx-

M003, Onset) connected to a data logger (U300-NRC, Onset) and installed 1m above the plants in the greenhouse. The 19 plants were randomly installed in the three rows in a mini-lysimeter greenhouse phenotyping platform (Bord'O platform, INRAE Bordeaux), alternating the cultivar, on individual scales (CH15R11, OHAUS type CHAMP) measuring their weight continuously during four months between 9 June and 1 October 2021. To avoid any water stress, plants were automatically watered to field capacity twice a day (at 8h and 20h). The field capacity was determined by immersing the plants into water for 15 minutes, draining, and then weighing the day before launching the experimentation. To measure only plant transpiration, the pots were sealed with bags during the whole experimentation.

Esca leaf symptom monitoring

Leaf symptom onset and evolution were monitored weekly over a three month-period at the leaf, current year shoot, and whole plant levels (Supplementary Fig. S1). At the end of the experimentation five out of nine 'Sauvignon blanc' and seven out of 10 'Cabernet Sauvignon' vines were symptomatic. The leaf symptoms were separated into three classes: "C", green leaves on control plants (asymptomatic between June and October 2021); "AS", green leaves from symptomatic plants (both before and after symptom appearance), and "S", symptomatic leaves (presenting tiger-stripe leaves) on symptomatic plants. Likewise, stems from control plants were named "C" and stems with symptomatic leaves "S".

Stem growth measurements

Stem diameter dynamics was continuously monitored on 11 vines randomly chosen (n = 6 'Sauvignon blanc' and n = 5 'Cabernet Sauvignon') using stem dendrometers (DD-S2 Dendrometer, Ecomatik). Plants were pruned to keep 4 spurs for each of the two arms, one bud for each spur was selected. Each dendrometer was installed on a randomly chosen stem

among the eight stems, on the first basal internode that was long and strong enough to support it. Trunk radial growth was also measured in four vines using trunk dendrometers installed in the middle part of the trunk. All dendrometers were connected to data-loggers (DL-18, Dendrometer data logger, Ecomatik) and the data were retrieved weekly via the HOBOWare software. Data were recorded on a 60-min schedule continuously from end-June to end-September. The raw dendrometer data of each vine were checked and cleaned using the "treenetproc" package via the R software (version 4.2.2) and its three main steps and functions. At the end of this cleaning procedure and as the dendrometers are placed at the beginning of the season without knowing the stem symptomatic evolution, the growth analysis had to be performed on one control and four symptomatic 'Cabernet Sauvignon' stems, and three control and three symptomatic 'Sauvignon blanc' stems.

Different growth parameters were calculated for different time intervals: (1) the maximum diameter of a day (MXD , in μm) which was normalised by the first value measured by the dendrometer to obtain comparable, size-independent measurements of dimensional changes (as done by Scholz *et al.*, 2008); (2) the daily growth rate (DGR , in μm) which is the difference between the maximum diameter between two consecutive days; (3) the weekly average DGR (DGR_w , in μm). Based on the patterns of DGR_w over the season and literature (Van de Wal *et al.*, 2018), and for further analysis, we separated the growing season in 3 periods: the stem growth period (before week 29, "GR"); the shrinkage period (between week 30 and 33, "SH"), and the stabilization at the end of the growing season (between week 34 and 39, "ST").

Xylem anatomy analysis

Stem cross-sections. At the end of the experimentation, one stem per plant that was not equipped with any dendrometers was selected (symptomatic stems from esca symptomatic

plants and asymptomatic stems from control plants). Xylem anatomy analysis was then performed on three control and five symptomatic ‘Sauvignon blanc’ stems and three control and six symptomatic ‘Cabernet Sauvignon’ stems. All stems had a maximum percentage of symptomatic leaves above 55%, except one ‘Sauvignon blanc’ stem with 27.8%. Among these stems, 42% produced green regrowth after symptom expression. One cm length samples from the 12th node from the base node were stored in 70% ethanol. Fifty μm thick stem cross sections were made using a GSL-1 microtome (Gärtner *et al.*, 2014). The sections were placed for about two minutes in a 0.5% safranin/astrablue solution, rinsed twice with absolute ethanol, impregnated with xylene, and then mounted between slide and coverslip with Histolaque (Histolaque LMR) to obtain permanent slides (three cross sections per sample). Pictures of the sections were taken using a binocular magnifier associated with a Nikon SMZ1270 camera, and the NIS-ElementsD software associated with the magnifier. For each sample, we selected the clearest, best colored, and most complete cross section for analysis.

Stem xylem analysis. The different anatomical traits measured and derived from these measurements for each sample are listed in Table 1 according to (Scholz *et al.*, 2013). In order to obtain a more accurate representation of the distribution of the fully or partially occluded vessels in the xylem according to the cultivar (‘Sauvignon blanc’, ‘Cabernet Sauvignon’) and the symptom (esca, control), an additional analysis was performed based on the relative position of each xylem vessel in the dorso-ventral region of each stem (Fig. 1). This process consisted in measuring the distance from the pith for each dorso and ventral vessel and analyzing continuously or in bins (of each 20% distance interval from the pith in the xylem tissue) the conduit characters (Table 1). The area for each stem portion was also measured to calculate vessel density.

Midrib cross-sections. Three “C”, four “S”, and four “AS” leaves were sampled in ‘Sauvignon blanc’ and three “C”, five “AS”, and six “S” leaves in ‘Cabernet Sauvignon’. One cm of the midrib of each leaf was stored in 70% ethanol. Samples were then fixed in a Formalin-Aceto-Alcohol (FAA) solution for 15h minimum and processed as described in details in (Bortolami *et al.*, 2023) with a dehydration phase followed by embedding using a graded series of LR White resin. Two μm cross sections were realized in each embedded sample using an ultracut S microtom (Reichert) equipped with a glass knife at the Bordeaux Imaging Center, a member of the France Bio Imaging national infrastructure (ANR-10-INBS-04). The sections were fixed to the slide by placing them on a warm plate and stained with 0.05% Toluidine blue O in order to detect the presence of tyloses and gels in the vessel lumens. Pictures of each section were taken using a binocular magnifier associated with a Nikon SMZ1270 camera, and the NIS-ElementsD software. For each slide, we selected the clearest, best colored, and most complete cross-section for analysis.

Midrib xylem analysis. Using imageJ software (Image J 1.53t, Wayne Rasband and contributors National Institutes of Health), the number of occluded and non-occluded vessels were counted in order to obtain a percentage of vessel occlusion per midrib.

Balance data analysis

The whole-plant transpiration per leaf area (E in $\text{mmol m}^{-2} \text{s}^{-1}$) was calculated as follows:

$$E = \frac{\Delta_w}{A_L} \times \frac{1}{MW_w}, \quad (1)$$

where Δ_w corresponds to the change in weight within the considered period (g s^{-1}), A_L to the total leaf area of the plant (m^2), and MW_w to the molecular weight of water (18 g mol^{-1}). To

avoid aberrant values, Δ_w measurements were considered only when ranging from 0 to -0.5 g s^{-1} which correspond to E values that lie within a reasonable range.

The total leaf area (A_L) was estimated through the relationship obtained between the leaf midrib length and the leaf area (measured with a leaf area meter Model LI-3000, LI-COR) for both cultivars using ~150 non-symptomatic leaves per cultivar. The leaf midribs were measured every other week on all the leaves of each plant. In the case of symptomatic plants, the green regrowth presence was noted and included in the total leaf area. The whole plant (canopy) conductance (G_C in $\text{mmol m}^{-2} \text{ s}^{-1}$), was then calculated as:

$$G_C = K_G(T) \times \frac{E}{D}, \quad (2)$$

where $K_G(T)$ corresponds to the conductance coefficient ($115.8 + 0.4236 \cdot T$, $\text{kPa m}^3 \text{ kg}^{-1}$), E to the transpiration (E in $\text{mmol m}^{-2} \text{ s}^{-1}$), and D to the vapor pressure deficit (kPa) calculated using relative humidity (in %) and T (in $^{\circ}\text{C}$) from climatic records. The G_C values were only used when radiation was saturating for photosynthesis (photosynthetic photon flux density (PPDF) $>700 \text{ } \mu\text{mol m}^{-2} \text{ s}^{-1}$) and when $D \geq 0.6 \text{ kPa}$ (Ewers and Oren 2000). In addition, errors in G_C estimates were kept to less than 10%.

Water potential

The minimum leaf water potential (between 13h and 15h) was measured weekly on mature well-exposed leaves from the middle of the stem, between June and September (12 measuring dates) with a pressure chamber (Scholander). For symptomatic plants, the water potential was measured only in AS leaves, to avoid an artifact measurement due to the occlusions of vessels by tyloses.

Gas exchange

Gas exchange measurements were realized between 9h and 12h on mature well-exposed leaves using the TARGAS-1 portable photosynthesis system (PP Systems). Optimal conditions of photosynthetic active radiation were set in the cuvette ($1,500 \mu\text{mol m}^{-2} \text{s}^{-1}$). The maximal CO_2 assimilation, A_{max} ($\mu\text{mol m}^{-2} \text{s}^{-1}$) was recorded on one (or two for symptomatic plants: “AS” and “S”) mature well-exposed leaf from the middle of the stem and by alternating the grape cultivars. The measurements were performed weekly on each of the 19 plants, for 10 measuring dates, between the 16 June and the 17 August 2021, gathering together 62 “C” leaves, 42 “S” leaves and 29 “AS” leaves.

The ambient stomatal conductance was measured weekly between the 21 July and the 22 September 2021, with the Li-600 (Licor) on the green surface of asymptomatic and symptomatic mature well-exposed leaves. The measurements were performed between 10h and 12h on each of the 19 plants, for 10 measuring dates, gathering together 69 control leaves from control asymptomatic plants, 79 symptomatic and 36 green asymptomatic leaves from symptomatic plants.

Statistical Analysis

DGR_W was analysed using a linear mixed-effects model with the plant parameter set as a random effect while the period (GR, SH, ST), the esca symptoms (control, esca) and their interactions as fixed effects. A post-hoc Tukey test adjustment for multiple comparisons was also realized. We only performed statistical analysis for ‘Sauvignon blanc’ DGR_W values as only one control stem could be monitored in ‘Cabernet Sauvignon’.

Anatomical characteristics of stem xylem and the percentage of occluded vessels in stems and midribs were compared between control plants of the two cultivars, and between control and symptomatic plants within each cultivar, using ANOVAs. We performed Levine's test to verify the equality of the variance. The vessel diameter curves were obtained by using the loess smoothing method.

The vessel density ($V_{D \text{ occ. vessels}}$ and $V_{D \text{ non occ. vessels}}$), the vessel size distribution, the theoretical specific hydraulic conductivity ($k_{ts \text{ all vessels}}$, $k_{ts \text{ non occ. vessels}}$ and $k_{ts \text{ occ. vessels}}$) and the PLC_{th} were analysed using linear mixed-effects models with the plant entered as a random effect, and the percentage distance interval from the pith ([0,20], (20,40], (40,60], (60,80] and (80,100]), the esca symptoms (control, esca), the cultivar ('Sauvignon blanc', 'Cabernet Sauvignon') and their interactions as fixed effects. The data were log transformed after examining residual plots. For data with significant zero we used the function \log_{1p} (package SparkR) to carry out the transformation. Leaf gas exchange (g_s and A) and midday water potentials were analyzed with linear mixed-effects models with the plant entered as a random effect, since several measurements were performed on the same plant over the season, and the cultivar, esca symptoms, and their interactions entered as fixed effects. A post-hoc Tukey test adjustment for multiple comparisons was realized. Whole-plant stomatal conductance (G_C) curves were obtained by using the loess smoothing method. All statistical analyses were performed using R (version 4.2.2) and are presented in Supplementary Tables S1 to S8.

RESULTS

Esca leaf symptom incidence

During the course of the experiment, five 'Sauvignon blanc' and seven 'Cabernet Sauvignon' plants exhibited esca leaf symptoms, with first symptom expression occurring between 5 July and 2 August 2021. The maximum percentage of symptomatic leaves for these plants ranged

from 27.7% to 100% per plant, with at least one stem per plant showing more than 75% leaf symptoms. The remaining four ‘Sauvignon blanc’ and three ‘Cabernet Sauvignon’ plants remained asymptomatic, and showed no esca leaf symptoms.

Growth and stem diameter variation

Regardless of the cultivar, stem diameter variation from control plants (C1, C2, C3, and C4 stems, Fig. 2, left panel) followed the same growth evolution. The first period is characterized by a fast increase of the *MXD* with time, occurring at the beginning of the growing season, until the stems reach a maximum diameter (ΔD_{max}) at the end of July (Fig. 2). The control ‘Cabernet Sauvignon’ stem reached ΔD_{max} on the 1st of August, 2021 (1088.72 μm , C1, Fig. 2, left panel). ‘Sauvignon blanc’ ΔD_{max} values ($n = 3$ stems, C2, C3, C4, Fig. 2, left panel) were lower than the ‘Cabernet Sauvignon’ stem and staggered between the 22th of July (580.64 μm , C3, Fig. 2, left panel) and the 28th of July (713 μm , C2, the maximum value in ‘Sauvignon blanc’ control plants, Fig. 2, left panel). The second period is characterized by a decrease of the *MXD* with time until ΔD_{max} stabilized in the third period of the growing season.

In contrast, after the growth period, the timing, length, and intensity of the shrinkage period was highly irregular from one symptomatic stem to another, deviating from the consistent pattern observed in control stems (Fig. 2). In two plants (S6 and S7; Fig. 2, right panel), several periods of shrinkage were observed. In others (e.g. S2, S3, and S5; Fig. 2, right panel), ΔD_{max} was observed later or the maximum stage was prolonged, S1 had no shrinkage period, and finally, the stem S4 presented the same pattern as the controls (Fig. 2, left and right panel).

The small number of reliable trunk dendrometers does not allow conclusions about the growth response of the trunk ($n = 1$ control and $n = 3$ symptomatic plants; Supplementary Fig. S2). However, we observed similar patterns between trunk and stem growth responses. For example, plant S1 increased in growth at the end of the season in both stem and trunk organs. A stall in the growth of both the stem and trunk of plant S5 was also observed, thus reinforcing the fact that this observation did not result from a measurement artifact. Finally, the only exploitable control trunk dendrometer (C2, Supplementary Fig. S2, left panel) showed the same growth pattern as the control stems characterized by the three phases of growth, shrinkage, and finally stabilization. Comparing the trunk and stem curves of the control plant (C2), we found a bigger and longer growth phase in the trunk as well as a later transition to the shrinkage phase (mid-August in the stem, end of August in the trunk).

Growth rate dynamic over the season

The three growth periods were precisely defined using the evolution of DGR_W over time in control stems (Fig. 3): positive DGR_W values were associated with the GR period (before the week 29); negative values with the SH period (between week 30 and 33), and values close to zero at the stabilization at end of the season (“ST”, between week 34 and 39).

Overall, the DGR_W dynamic over the season was visually similar between cultivars, despite higher values during the GR period in ‘Cabernet Sauvignon’ (Fig. 3). In ‘Sauvignon blanc’, the period and the interaction between period and the esca symptoms, have a significant impact on DGR_W (Supplementary Table S1). The DGR_W of control and symptomatic plants did not significantly differ during the GR and ST periods (Fig. 3; $P > 0.05$, Tukey test). However, during the SH period, the DGR_W of control stems was significantly lower (*i.e.*

higher shrinkage) than that of symptomatic stems (Fig. 3(i); $P = 0.01$). The same trend was observed in ‘Cabernet Sauvignon’ even if only one control stem could be monitored.

Xylem anatomical analysis

Stem xylem anatomy

Among control plants, the pith area (PA), xylem area (A_x), and the vessel density (V_D) did not differ significantly between cultivars (Supplementary Table S2). Hydraulic diameter was significantly higher in ‘Sauvignon blanc’ ($D_H = 153.5 \pm 13.3 \mu\text{m}$) than in ‘Cabernet Sauvignon’ ($D_H = 84.5 \pm 12.2 \mu\text{m}$), resulting in a four times higher theoretical hydraulic conductivity (k_{ts}) in ‘Sauvignon blanc’ control stems (Supplementary Fig. S3, Supplementary Table S2).

Symptomatic and control stems did not present significant differences in PA , A_x , V_D , D_H , k_{ts} in ‘Cabernet Sauvignon’ and ‘Sauvignon blanc’ for whole stem section analyses (Supplementary Table S2).

Vessel occlusion in stems and midribs

The percentage of vessels occluded by tyloses or gels was quantified on stem and midrib cross sections and was lower than 4% in control stems and midribs of the two cultivars (Fig. 4). In symptomatic stems, $9.6\% \pm 1.8$ of xylem vessels were occluded in ‘Cabernet Sauvignon’ and $25.6\% \pm 10.8$ in ‘Sauvignon blanc’ (Fig. 4A). However, the differences in % vessel occlusion between control and symptomatic stems within each cultivar was not significant (Fig. 4A). It can be noted that when selecting only stems with more than 55% of symptomatic leaves (i.e. removing one stem with 27% of symptomatic leaves), the percentage of occluded vessels was significantly higher than that of the control stems in

‘Sauvignon blanc’ ($P = 0.03$, Kruskal Wallis). At the leaf level, midribs of symptomatic leaves had significantly more occluded vessels than asymptomatic and control leaves in both cultivars (Fig. 4B).

Anatomical trait variability across the xylem area

Vessel density (V_D)

Vessel density of occluded vessels, $V_{D \text{ occluded vessels}}$, significantly differed between intervals across the xylem area and was the greatest closest to the pith (0-20% distance from the pith) in both symptomatic and control plants (Fig. 5, Supplementary Table S3). Moreover, the $V_{D \text{ occluded vessels}}$ significantly differed between symptomatic and control plants (Supplementary Table S3). Indeed, $V_{D \text{ occluded vessels}}$ in symptomatic stems was higher than that of controls in all intervals in ‘Sauvignon blanc’, and especially in the first two intervals in ‘Cabernet Sauvignon’ (Fig. 5A).

Vessel density of non-occluded vessels, $V_{D \text{ non occ. vessels}}$, significantly differed between intervals across the xylem area in control as well as in symptomatic stems (Supplementary Table S3). $V_{D \text{ non occ. vessels}}$ was the highest closest to the pith and in the outermost xylem interval in both control and symptomatic plants, regardless of the cultivar (Fig. 5B). Furthermore, we found a significant effect of the interaction between plant symptoms and intervals across the xylem area on $V_{D \text{ non occ. vessels}}$. In the outermost xylem interval, the $V_{D \text{ non occ. vessels}}$ in esca symptomatic stems was 105% higher than in control stems in ‘Sauvignon blanc’ (despite marginally significant differences, $P = 0.05$, Kruskal Wallis) and 184% higher in ‘Cabernet Sauvignon’ ($P = 0.07$, Kruskal Wallis) (Fig. 5B).

Distribution of vessel size

The distribution of vessel diameter across the xylem area significantly varied according to the cultivar, esca symptom expression, and distance to pith (Supplementary Table S4). Overall, xylem vessel diameters of ‘Cabernet Sauvignon’ stems were significantly smaller than those of ‘Sauvignon blanc’ stems (Fig. 6). In particular, in control stems the mean vessel diameter was $44.6 \pm 0.9 \mu\text{m}$ in ‘Cabernet Sauvignon’ versus $58.4 \pm 1.4 \mu\text{m}$ in ‘Sauvignon blanc’ and in symptomatic stems $36.8 \pm 0.5 \mu\text{m}$ in ‘Cabernet Sauvignon’ versus $48.2 \pm 0.8 \mu\text{m}$ in ‘Sauvignon blanc’. The vessels with the smallest diameters were located near the pith and in the outermost interval in control plants (Fig. 6). In ‘Sauvignon blanc’, vessels from symptomatic plants were significantly smaller than those of control ‘Sauvignon blanc’ plants, especially in the last 50% distance from the pith. In ‘Cabernet Sauvignon’, vessels were in the same range of size in symptomatic and control stems until the last 30% distance from the pith, where the vessels were smaller in symptomatic stems (Fig. 6).

Theoretical specific hydraulic conductivity

The k_{ts} all vessels (including occluded and non-occluded vessels) and the k_{ts} non occ. vessels significantly differed between intervals across the xylem area, depending on the cultivar (significant interactions between xylem interval and cultivar, as presented in Supplementary Table S5). In ‘Sauvignon blanc’, the k_{ts} all vessels and k_{ts} non occ. vessels visually increased towards the interval 60 to 80% distance from the pith, before decreasing in the most exterior portion of the xylem tissue, particularly in the control stems (Fig. 7A; Supplementary Fig. S4A). In ‘Cabernet Sauvignon’, k_{ts} all vessels was visually consistent across xylem intervals and was significantly lower than in ‘Sauvignon blanc’ (Fig. 7A; Supplementary Table S5). The k_{ts} all vessels and k_{ts} non occ. vessels did not display significant differences between control and

symptomatic plants (Supplementary Table S5). Yet, in symptomatic stems of ‘Sauvignon blanc’, k_{ts} tended to be lower (the maximum values of k_{ts} all vessels were 33% lower in esca symptomatic plants than that of control plants; Fig. 7A; Supplementary Fig. S4A).

The k_{ts} occ. vessels (i.e. corresponding to the theoretical loss of conductivity as also analysed with the PLC_{th} below) was significantly different between intervals and between control and symptomatic plants with higher values in symptomatic ‘Sauvignon blanc’ in all intervals and in the first two intervals in the ‘Cabernet Sauvignon’ (Supplementary Fig. S4B, Supplementary Table S5).

Theoretical percentage loss of conductivity (PLC_{th})

The distribution of PLC_{th} across the xylem tissue intervals significantly differed between control and symptomatic stems (Fig. 7B, Supplementary Table S6). In ‘Sauvignon blanc’, PLC_{th} was greater in symptomatic plants than controls in all intervals and was distributed in a parabolic way (the maximum was $9.2\% \pm 4.9$ at the interval (40,60] and the minimum was $4.3\% \pm 3.2$ at the outermost intervals). ‘Cabernet Sauvignon’ symptomatic stems were characterized by a more localized loss of conductivity within the xylem at the [0,60] interval. Very low levels of PLC_{th} were observed in the outermost intervals of symptomatic ‘Cabernet Sauvignon’ stems. The highest PLC_{th} in ‘Cabernet Sauvignon’ controls was localized at the [0,20] interval ($3.6 \pm 2.3\%$).

In whole cross-sections, the theoretical percentages loss of conductivity (PLC_{th} all section) was lower in symptomatic stems compared to control ones in both varieties but not significantly (Fig. 7B (i and ii)). Indeed, in ‘Sauvignon blanc’, the PLC_{th} all section was $0.8\% \pm 0.5$ in control and $31.9\% \pm 15$ in symptomatic stems (Fig. 7B (i)) In ‘Cabernet Sauvignon’ the PLC_{th} all section was $3.4\% \pm 2.4$ in control and $16.9\% \pm 6.8$ in symptomatic stems (Fig. 7B (ii)).

Water relation at leaf and whole plant scale

In both cultivars, the whole plant stomatal conductance (G_C) of control plants was relatively stable until the beginning of August and then decreased at the end of the season (Supplementary Fig. S5). Overall, G_C of ‘Cabernet Sauvignon’ control plants was lower than that of ‘Sauvignon blanc’ on average (Supplementary Fig. S5).

In symptomatic plants, a decrease in G_C was observed in both cultivars several days prior to the appearance of esca leaf symptoms (necrosis of secondary veins and discoloration of the leaf blade, potentially linked to tissue death). The average daily minimum G_C was reached 8 days after the first symptom observation in ‘Cabernet Sauvignon’ and 15 days after in ‘Sauvignon blanc’. An increase in G_C was then observed three weeks after the first symptom observation in ‘Sauvignon blanc’ (Fig. 8A). The G_C of ‘Cabernet Sauvignon’ stabilized after 1 week until the end of the season (Fig. 8A).

No significant differences between cultivars were found in CO_2 assimilation (A_{max}) and the stomatal conductance (g_s) (Supplementary Table S7, Fig. 8B-C). Green leaves from symptomatic and control plants (AS and C leaves, respectively) presented similar levels of gas exchange (Supplementary Table S7, Fig. 8B-C). The symptomatic leaves presented a significantly lower stomatal conductance (g_s) and maximal CO_2 assimilation (A_{max}) than apparently healthy leaves (C and AS) (Supplementary Table S7, Fig. 8B-C). Midday leaf water potentials were measured along the season on green leaves (water potentials cannot be measured on symptomatic leaves because their xylem vessels are occluded) and did not significantly differ between leaf symptoms and cultivar (Supplementary Table S8, Supplementary Fig. S6).

DISCUSSION

In this study we investigated the relationships between stem growth dynamics, physiology, and xylem anatomy during esca pathogenesis in two susceptible grapevine cultivars, ‘Sauvignon blanc’ and ‘Cabernet Sauvignon’. In both cultivars, we demonstrated that esca pathogenesis resulted in an alteration in stem growth patterns associated with xylem occlusions in leaves and stems, theoretical loss of conductivity, and a change in stem cambial activity with the production of small functional vessels at the end of the season. Finally, we highlighted that the pathogenesis of esca and varietal differences in xylem anatomy affect gas exchange at both leaf and whole-plant levels. We found a recovery in whole plant stomatal conductance two weeks after symptom onset in ‘Sauvignon blanc’ and a stabilization after one week in ‘Cabernet Sauvignon’. These results shed light on the resilience mechanisms of symptomatic vines, which drive the production of new green leaves and shoots after symptom onset.

Esca leaf symptoms alter stem growth dynamics

Plant growth responses to abiotic stresses, particularly the response of radial growth of stems and trunks to drought stress, are well-studied (Daudet *et al.*, 2005; Fernández and Cuevas 2010). On the contrary, studies focused on the influence of vascular disease on seasonal growing patterns are rare (but see Cohen *et al.*, 1997). Radial dendrometers which continuously measure stem or trunk diameters are ideal for monitoring plant growth in real time (Deslauriers *et al.* 2007). Here we observed the typical pattern of maximum daily diameter (*MXD*) evolution over the season in the control plants (successively a growth, a shrinkage, and a stabilization period; Fig. 2) (Intrigliolo and Castel 2007; Van de Wal *et al.*, 2018; Conesa *et al.*, 2018). Additionally it is important to note that the growth pattern of control plants doesn’t appear to be affected by the absence of grape berries, as demonstrated

by (Van de Wal *et al.*, 2018). Conversely, esca pathogenesis had a significant impact on stem growth patterns. Esca systematically perturbs growth dynamics when compared to the control pattern. Depending on the plant, the shrinkage phase can occur at the same time or later as in control plants, can be absent or can be observed multiple times over the season. The average growth rate during the shrinkage period (“SH”, based on the control plants) was significantly higher in the ‘Sauvignon blanc’ symptomatic plants (only one control stem was monitored in ‘Cabernet Sauvignon’). One of the biggest difficulties in studying esca is that it is impossible to know at the beginning of the season which plants or stems will express symptoms and when. This explains, especially in the dendrometer analysis, the different sample sizes of control and symptomatic plants. Although we were able to use only a small number of trunk dendrometers, we observed similar trunk radial growth patterns as in stems (Supplementary Fig. S2).

The observed alteration in stem growth patterns were observed at a distance from the trunk where the esca-related pathogens are living (Bortolami *et al.*, 2019). In other perennial species, a reduction in growth has been observed after inoculation with different pathogens (Cohen *et al.*, 1997; Luque *et al.*, 1999), differing from our study by the proximity of the inoculation site to the position of the sensor used (placed 15 cm above). These authors also showed that the evolution of growth after inoculation was pathogen-dependent. The heterogeneous growth response we observed in symptomatic plants could be due to the fact that several esca-related pathogen species are associated with esca symptoms and/or to the heterogeneity of plant responses to their interactions with pathogens.

Xylem development adaptation during esca pathogenesis

The decrease in growth following pathogen inoculation (or in our case, pathogen activity) could result from the occlusion of xylem vessels as suggested by (Luque *et al.*, 1999) and

(Cohen *et al.*, 1997). The pathogenesis of plant diseases can be associated with anatomical changes in wood, especially in terms of vessel diameter, density and tylose production over years (Renzi *et al.*, 2012; Sabella *et al.*, 2020). To understand the alteration of the shrinkage period during esca pathogenesis, we explored the anatomical characteristics of stem xylem, specifically by categorizing the different types of vessels observed in xylem sectors from the pith to the outer part of the xylem.

Overall, symptomatic stems had a slightly higher percentage of tyloses (i.e. xylem occlusions) than control stems, and a significantly higher density of occluded vessels. This finding confirms previous results found in esca-symptomatic ‘Sauvignon blanc’ (Bortolami *et al.*, 2021a) and in other vascular pathogenesis, such as Pierce’s disease caused by *Xylella fastidiosa* (Sun *et al.*, 2013; Fanton *et al.*, 2022). By dividing the dorso-ventral region of each stem into five intervals based on the distance from the pith, we conducted a more detailed spatial analysis of vessel density and diameter, as well as k_{ts} , and PLC_{th} . We demonstrated that tylosis formation in control plants was low and restricted to the closest interval to the pith (i.e. protoxylem), where the vessels are predominantly small in size, less than fifty μm . On the contrary, in esca-symptomatic stems, the density of occluded vessels was higher than in control stems in all intervals across the xylem area, suggesting a plant defense response.

Interestingly, symptomatic plants were able to produce non-occluded vessels late in the season (see examples in Supplementary Fig. S1), efficiently transporting sap as shown by dye infiltration (Fig. 4(i)). Those vessels, observed above 60% of the relative distance from the pith, were much smaller and in a higher density than vessels of control plants in the same xylem sector. The production of numerous small vessels in the xylem periphery has also been identified in the case of the Flavescence dorée disease on the tolerant cultivar ‘Merlot’ and not on the susceptible cultivar ‘Chardonnay’ (Jelmini *et al.*, 2021). In the context of abiotic

stress (e.g. drought), the decrease in stem basal area during drought and then its increase post-drought has already been associated with “hydraulic repair” in response to embolism via the formation of new functional vessels in woody trees such as *Callitris* (Brodrribb *et al.*, 2010) and *Eucalyptus* (Gauthey *et al.*, 2022). This suggests that after a drought, the cambium had the capacity to produce new vessels. In these two cases of biotic and abiotic stress, it appears that the ability to produce new vessels and thus new shoots helps to maintain productivity and enhance the likelihood of survival. This suggests that the alteration of the shrinkage phase during esca pathogenesis may be related to the preservation of a cambial activity. Here, the formation of numerous small functional xylem vessels at the end of the season may have supported the formation of new healthy shoots, and compensated for the negative consequences of esca on plant growth dynamics, physiology and xylem anatomy. The hypothesis of the positive influence of new green shoots on plant health is supported by previous research showing that esca did not negatively impact stem starch content in winter in untopped esca-symptomatic vines (Bortolami *et al.*, 2021b). Vessel occlusion by tylosis is a phenomenon associated with ethylene production (Sun *et al.*, 2007). This gaseous phytohormone, sometimes in association with other hormones such as auxin, stimulates cambial activity by acting through ethylene receptors (Sorce *et al.*, 2013). Future research could aim to study the importance of ethylene and the causal relationships between tylosis formation, growth alteration, and the preservation of vessel formation.

Differential impact of esca on grapevine hydraulics among cultivars

Vessel size partly determines the plant water-carrying capacity by conditioning the hydraulic conductivity (Tyree and Zimmermann 2002). Hydraulic traits have been reported between cultivars (Dayer *et al.*, 2020; Villalobos-González *et al.*, 2018) and also during the development of vascular diseases (Sun *et al.*, 2013; Bortolami *et al.*, 2021a). Additionally,

studies have demonstrated that cultivar variability can result in heterogeneous responses of hydraulic traits in the presence of a vascular pathogen (Deyett and Rolshausen 2019; Fanton and Brodersen 2021).

In our study, we showed that the k_{ts} differed according to the grape cultivar, with a reduced k_{ts} ($k_{ts \text{ all vessels}}$ and $k_{ts \text{ non occ. vessels}}$) in 'Cabernet Sauvignon'. In addition, the development of esca led to a significantly higher theoretical percentage loss of conductivity (PLC_{th}) due to vessel occlusions in symptomatic stems than in control stems across intervals. The theoretical impact of vessel occlusions was also evidenced through a significantly higher $k_{ts \text{ occ. vessels}}$ in symptomatic stems than in control stems. However, we did not identify any significant difference in k_{ts} ($k_{ts \text{ all vessels}}$ and $k_{ts \text{ non occ. vessels}}$) between symptomatic and control plants in either of the two grape cultivars. This can be explained by the variability in the percentage of occlusion in stem xylem vessels (Deyett and Rolshausen 2019; Fanton and Brodersen 2021). In addition, fifty μm cross-sections at a given vertical location in each section were analysed and we can assume that, in the case of symptomatic plants, some of the vessels defined as non-occluded may be actually occluded up- or down-stream. Therefore, it is likely that we overestimated the contribution of non-occluded vessels to $k_{ts \text{ non occlu. vessels}}$ and underestimated the compensatory effect of late functional vessel production. Tyloses occluding stem xylem vessels are responsible for hydraulic conductivity losses as shown for example in a root pathogen infecting pine trees (Mensah *et al.*, 2020, and in esca disease Bortolami *et al.*, 2021a).

At the leaf level, we confirmed that esca symptoms are associated with significant levels of vessel occlusion in both cultivars (as also shown by Bortolami *et al.*, 2023). However the impact of these occlusions on gas exchange was still unclear. At the leaf level, we showed that leaf symptom onset was associated with a decrease in stomatal conductance and CO_2

assimilation in both cultivars. At the whole-plant level, we demonstrated that the onset of leaf symptoms was preceded by a decrease in canopy conductance (G_C), in both ‘Sauvignon blanc’ and ‘Cabernet Sauvignon’. This pattern was previously shown in ‘Sauvignon blanc’ by (Bortolami *et al.*, 2021b), confirming the negative impact of esca on whole-plant gas exchange. We also confirmed that esca did not affect midday water potential and gas exchanges in asymptomatic leaves in either of the two cultivars, despite significant losses of conductivity in stems. The damage responsible for causing reductions in G_C is thus primarily localized within the symptomatic leaves. Both cultivars were able to produce new green leaves after pathogenesis, and we can link this capacity with the observed recovery of G_C in ‘Sauvignon blanc’ and the G_C stabilization in ‘Cabernet Sauvignon’. This formation of new healthy shoots and G_C recovery may have been supported by the maintenance of cambial activity through the formation of numerous small functional xylem vessels at the end of the season. Symptomatic stems exhibit a certain degree of resilience to the disease, whereas leaves, crucial for growth, cannot recover and eventually die.

To conclude, we showed that esca pathogenesis altered the shrinkage phase during stem growth, likely through modified vascular cambial activity. Symptomatic plants were able to compensate for the negative impacts of esca on leaves, especially on stomatal and canopy conductance. We hypothesize that stem xylem occlusions and the subsequent localized loss of conductivity in the symptomatic stems could trigger the production of new numerous small xylem vessels associated with new healthy shoots at the end of the season. These results suggest that grapevine has resilience mechanisms that could play a crucial role in its defense against esca. The mechanisms underlying the modification of cambial activity during esca pathogenesis are still unknown and are a promising area for further research. To go further, it would be essential to study these responses on a wider range of grape cultivars more or less sensitive to this disease in similar contexts. Comparing different levels of plant vigor, either

in the field or in potted plants, could also be an important field of research to investigate vigor impact on resilience capacity. In cultivated vineyards, topping is a common procedure used several times during the year to maintain a constant vegetative surface and to allow the passage of vineyard machinery. However, in a vineyard highly infected by esca, this practice could play a negative role by removing new photosynthetically active "organs" produced by the symptomatic plants in the weeks following symptom development, thus preventing a recovery of gas exchange and photosynthetic activity that contribute to the maintenance of carbohydrate reserves.

Accepted Manuscript

ACKNOWLEDGMENTS

We thank the experimental teams of UMR SAVE and UMR EGFV (INRAE, Bordeaux, France) for providing the materials, logistics and assistance during the experimentation. We thank Jérôme Jolivet and Sebastien Gambier (UMR SAVE) for providing technical knowledge and support for plant transplantation and maintenance. We thank Nabil Girollet, Guillaume Pacreau, and Nabil Zirari for the maintenance of the mini-lysimeter greenhouse phenotyping platform (Bord'O platform, INRAE Bordeaux). We thank Régis Burlett and Patrick Leger for the dendrometer's expertise, support and materials. This work was supported by the projects PHYSIOPATH (22001150) and ESCAPADE (22001436) (program “Plan National Dépérissement du Vignoble”, FranceAgriMer/CNIV) and the Nouvelle-Aquitaine region (project VITIPIN, 22001439).

CONFLICT OF INTEREST

The authors declare that they have no competing interests in relation to this study.

AUTHOR CONTRIBUTIONS

C.E.L.D., G.A.G., N.D.A., S.D., L.L., N.S. designed the experiments;

N.D.A., C.E.L.D., and N.F. conducted the esca symptom notations;

N.D.A. and N.F. carried out the samplings, manage the dendrometers over the season; measured leaf gas exchange and leaf area;

N.D.A., N.F., C.E.L.D measured midday water potentials;

P.T. and N.F. conducted the histological preparation;

N.D.A. and P.T. processed the optical images on ImageJ;

N.D.A. analyzed optical images and data sets from balances, leaf areas, dendrometers, weather stations, leaf gas exchange, and water potentials;

N.D.A., C.E.L.D., and G.A.G. wrote the article;

all authors edited and agreed on the last version of the article.

DATA AVAILABILITY

We agree to archive the data associated with this manuscript should the manuscript be accepted.

SUPPORTING INFORMATION

Supplementary data are available online at <https://academic.oup.com/aob> and consist of the following.

Fig. S1. Photographs of whole plants, leaves, and cross sections of esca-symptomatic or control plants of *Vitis vinifera* cv. ‘Sauvignon blanc’ and ‘Cabernet Sauvignon’.

Fig. S2. Evolution of the standardised maximum daily diameter (*MXD* in μm) of different trunks, during one vegetative season, in *Vitis vinifera* cv. ‘Sauvignon blanc’ and ‘Cabernet Sauvignon’.

Fig. S3. Stem xylem anatomy in *Vitis vinifera* cv. ‘Sauvignon blanc’ and ‘Cabernet Sauvignon’ control plants.

Fig. S4. Relationships between theoretical specific hydraulic conductivity and normalised distance to the pith (%) in symptomatic and control stems of ‘Sauvignon blanc’ and ‘Cabernet Sauvignon’, when considering either non-occluded vessels (A) or occluded vessels (B).

Fig. S5. Evolution of the whole plant (canopy) stomatal conductance (G_C , $\text{mmol m}^{-2} \text{s}^{-1}$) of control plants during the season in *Vitis vinifera* cv. ‘Sauvignon blanc’ and ‘Cabernet Sauvignon’.

Fig. S6. Midday water potentials measured on different types of ‘Sauvignon blanc’ and ‘Cabernet Sauvignon’ leaves.

Table S1. Effect of esca leaf symptoms and growth period (GR, SH, ST) on the average weekly daily growth rate (DGR_W) in ‘Sauvignon blanc’.

Table S2. Comparative analysis of xylem anatomical characteristics in ‘Sauvignon blanc’ and ‘Cabernet Sauvignon’ control stems, and in control and esca symptomatic stems within each cultivar using ANOVAs.

Table S3. Effect of the normalised distance from the pith, cultivar, and esca leaf symptoms on vessel density (V_D , estimated from non-occluded vessels and occluded vessels).

Table S4. Effect of the normalised distance from the pith, cultivar, and esca leaf symptoms on vessel size.

Table S5. Effect of the normalised distance from the pith, cultivar, and esca leaf symptoms on k_{ts} (estimated for all vessels, non-occluded vessels, and occluded vessels only).

Table S6. Effect of the normalised distance from the pith, cultivar, and esca leaf symptoms on the theoretical percentage loss of conductivity (PLC_{th}).

Table S7. Effect of cultivar and esca leaf symptoms on g_s and A .

Table S8. Effect of cultivar and esca leaf symptoms on midday water potentials.

Accepted Manuscript

REFERENCES

- Bortolami G, Farolfi E, Badel E, et al. 2021a.** Seasonal and long-term consequences of esca grapevine disease on stem xylem integrity. *Journal of Experimental Botany* **72**: 3914–3928. DOI: 10.1093/jxb/erab117.
- Bortolami G, Ferrer N, Baumgartner K, et al. 2023.** Esca grapevine disease involves leaf hydraulic failure and represents a unique premature senescence process. *Tree Physiology* **43**: 441–451. DOI: 10.1093/treephys/tpac133.
- Bortolami G, Gambetta GA, Cassan C, et al. 2021b.** Grapevines under drought do not express esca leaf symptoms. *Proceedings of the National Academy of Sciences of the United States of America* **118**. DOI: 10.1073/pnas.2112825118.
- Bortolami G, Gambetta GA, Delzon S, et al. 2019.** Exploring the hydraulic failure hypothesis of esca leaf symptom formation. *Plant Physiology* **181**: 1163–1174.
- Brodrribb TJ, Bowman DJMS, Nichols S, Delzon S, Burlett R. 2010.** Xylem function and growth rate interact to determine recovery rates after exposure to extreme water deficit. *The New Phytologist* **188**: 533–542. DOI: 10.1111/j.1469-8137.2010.03393.x.
- Bruez E, Lecomte P, Grosman J, et al. 2013.** Overview of grapevine trunk diseases in France in the 2000s. *Phytopathologia Mediterranea* **52**: 262–275. DOI : 10.14601/Phytopathol_Mediterr-11578.
- Cailleret M, Jansen S, Robert EMR, et al. 2017.** A synthesis of radial growth patterns preceding tree mortality. *Global Change Biology* **23**: 1675–1690. DOI: 10.1111/gcb.13535.
- Cohen M, Luque J, Alvarez IF. 1997.** Use of stem diameter variations for detecting the

effects of pathogens on plant water status. *Annales des Sciences Forestières* **54**: 463–472.

DOI: 10.1051/forest:19970504

Collins BR, Parke JL, Lachenbruch B, Hansen EM. 2009. The effects of *Phytophthora ramorum* infection on hydraulic conductivity and tylosis formation in tanoak sapwood.

Canadian Journal of Forest Research **39(9)**: 1766–1776. DOI: 10.1139/X09-097.

Conesa MR, Dodd IC, Temnani A, De la Rosa JM, Pérez-Pastor A. 2018. Physiological response of post-veraison deficit irrigation strategies and growth patterns of table grapes (cv. Crimson Seedless).

Agricultural Water Management **208**: 363–372. DOI:

10.1016/j.agwat.2018.06.019.

Daudet F-A, Améglio T, Cochard H, Archilla O, Lacoïnte A. 2005. Experimental analysis

of the role of water and carbon in tree stem diameter variations. *Journal of Experimental*

Botany **56**: 135–144. DOI: 10.1093/jxb/eri026.

Dayer S, Herrera JC, Dai Z, et al. 2020. The sequence and thresholds of leaf hydraulic

traits underlying grapevine varietal differences in drought tolerance. *Journal of Experimental*

Botany **71**: 4333–4344. DOI: 10.1093/jxb/eraa186.

De Micco V, Balzano A, Wheeler EA, Baas P. 2016. Tyloses and gums: A review of

structure, function and occurrence of vessel occlusions. *IAWA journal / International*

Association of Wood Anatomists **37**: 186–205. DOI: 10.1163/22941932-20160130.

Deslauriers A, Rossi S, Anfodillo T. 2007. Dendrometer and intra-annual tree growth: What

kind of information can be inferred? *Dendrochronologia* **25**: 113–124. DOI:

10.1016/j.dendro.2007.05.003.

Deyett E, Rolshausen PE. 2019. Temporal dynamics of the sap microbiome of grapevine

under high Pierce's disease pressure. *Frontiers in Plant Science* **10**: 1246. DOI: 10.3389/fpls.2019.01246.

Dixon HH, Joly J. 1894. On the ascent of sap. *Proceedings of the Royal Society of London* **57**: 3–5. DOI: 10.1126/science.179.4079.

Ewers B, Oren R. 2000. Analyses of assumptions and errors in the calculation of stomatal conductance from sap flux measurements. *Tree Physiology* **20**: 579–589. DOI: 10.1093/treephys/20.9.579.

Fanton AC, Brodersen C. 2021. Hydraulic consequences of enzymatic breakdown of grapevine pit membranes. *Plant Physiology* **186**: 1919–1931. DOI: 10.1093/plphys/kiab191.

Fanton AC, Furze ME, Brodersen CR. 2022. Pathogen-induced hydraulic decline limits photosynthesis and starch storage in grapevines (*Vitis sp.*). *Plant, Cell & Environment* **45**: 1829–1842. DOI: 10.1111/pce.14312.

Fernández JE, Cuevas MV. 2010. Irrigation scheduling from stem diameter variations: A review. *Agricultural and Forest Meteorology* **150**: 135–151. DOI: 10.1016/j.agrformet.2009.11.006.

Gärtner H, Lucchinetti S, Schweingruber F. 2014. New perspectives for wood anatomical analysis in dendrosciences: The GSL1-microtome. *Dendrochronologia* **32**: 47–51. DOI: 10.1016/j.dendro.2013.07.002.

Gauthey A, Peters JMR, Lòpez R, et al. 2022. Mechanisms of xylem hydraulic recovery after drought in *Eucalyptus saligna*. *Plant, Cell & Environment* **45**: 1216–1228. DOI: 10.1111/pce.14265.

Gruber A, Oberhuber W, Wieser G. 2018. Nitrogen addition and understory removal but not soil warming increased radial growth of *Pinus cembra* at treeline in the Central Austrian Alps. *Frontiers in Plant Science* **9**: 711. DOI: 10.3389/fpls.2018.00711.

Hartmann H, Messier C. 2008. The role of forest tent caterpillar defoliations and partial harvest in the decline and death of sugar maple. *Annals of Botany* **102**: 377–387. DOI: 10.1093/aob/mcn104.

Hofstetter V, Buyck B, Croll D, Viret O, Couloux A, Gindro K. 2012. What if esca disease of grapevine were not a fungal disease? *Fungal Diversity* **54**: 51–67. DOI: 10.1007/s13225-012-0171-z.

Intrigliolo D, Castel J. 2007. Evaluation of grapevine water status from trunk diameter variations. *Irrigation Science* **26**: 49-59. DOI: 10.1007/s00271-007-0071-2.

Jelmini L, Rizzoli A, Jermini M, Schumpp O, Conedera M. 2021. Phloem and xylem modifications of *Vitis vinifera* stems in response to flavescence dorée phytoplasma infection. *Plant Pathology* **70**: 970–979. DOI: 10.1111/ppa.13330

Luque J, Cohen M, Savé R, Biel C, Álvarez IF. 1999. Effects of three fungal pathogens on water relations, chlorophyll fluorescence and growth of *Quercus suber* L. *Annals of Forest Science* **56**: 19–26. DOI: 10.1051/forest:19990103.

McDowell NG, Sapes G, Pivovarov A, et al. 2022. Mechanisms of woody-plant mortality under rising drought, CO₂ and vapour pressure deficit. *Nature Reviews Earth & Environment* **3**: 294–308. DOI: 10.1038/s43017-022-00272-1.

Mensah JK, Sayer MAS, Nadel RL, Matusick G, Eckhardt LG. 2020. Physiological response of *Pinus taeda* L. trees to stem inoculation with *Leptographium terebrantis*. *Trees*

34: 869–880. DOI: 10.1007/s00468-020-01965-0.

Mugnai L, Graniti A, Surico G. 1999. Esca (black measles) and brown wood-streaking: Two old and elusive diseases of grapevines. *Plant Disease* **83**: 404–418. DOI: 10.1094/pdis.1999.83.5.404.

Oliva J, Stenlid J, Grönkvist-Wichmann L, et al. 2016. Pathogen-induced defoliation of *Pinus sylvestris* leads to tree decline and death from secondary biotic factors. *Forest Ecology and Management* **379**: 273–280. DOI: 10.1016/j.foreco.2016.08.011.

Pearce RB. 1996. Antimicrobial defences in the wood of living trees. *The New Phytologist* **132**: 203–233. DOI: 10.1111/j.1469-8137.1996.tb01842.x.

Renzi M, Copini P, Taddei AR, et al. 2012. Bacterial canker on kiwifruit in Italy: Anatomical changes in the wood and in the primary infection sites. *Phytopathology* **102**: 827–840. DOI: 10.1094/PHYTO-02-12-0019-R.

Rioux D, Nicole M, Simard M, Ouellette GB. 1998. Immunocytochemical evidence that secretion of pectin occurs during gel (gum) and tylosis formation in trees. *Phytopathology* **88**: 494–505. DOI: 10.1094/PHYTO.1998.88.6.494.

Rizzoli A, Jelmini L, Pezzatti G, et al. 2022. Impact of the “Flavescence Dorée” phytoplasma on xylem growth and anatomical characteristics in trunks of “Chardonnay” Grapevines (*Vitis vinifera*). *Biology* **11**: 978. DOI: 10.3390/biology11070978.

Rudelle J, Octave S, Kaid-Harche M, Roblin G, Fleurat-Lessard P. 2005. Structural modifications induced by *Eutypa lata* in the xylem of trunk and canes of *Vitis vinifera*. *Functional Plant Biology: FPB* **32**: 537–547. DOI: 10.1071/FP05012.

Sabella E, Moretti S, Gärtner H, et al. 2020. Increase in ring width, vessel number and $\delta^{18}\text{O}$ in olive trees infected with *Xylella fastidiosa*. *Tree Physiology* **40**: 1583–1594. DOI: 10.1093/treephys/tpaa095.

Scholz F, Bucci S, Goldstein G, Meinzer F, Franco A, Miralles- Wilhelm F. 2008. Temporal dynamics of stem expansion and contraction in savanna trees: Withdrawal and recharge of stored water. *Tree Physiology* **28**: 469–480. DOI: 10.1093/treephys/28.3.469.

Scholz A, Klepsch M, Karimi Z, Jansen S. 2013. How to quantify conduits in wood? *Frontiers in Plant Science* **4**: 56. DOI: 10.3389/fpls.2013.00056.

Sorce C, Giovannelli A, Sebastiani L, Anfodillo T. 2013. Hormonal signals involved in the regulation of cambial activity, xylogenesis and vessel patterning in trees. *Plant Cell Reports* **32**: 885–898. DOI: 10.1007/s00299-013-1431-4.

Sun Q, Rost TL, Reid MS, Matthews MA. 2007. Ethylene and not embolism is required for wound-induced tylose development in stems of grapevines. *Plant Physiology* **145**: 1629–1636. DOI: 10.1104/pp.107.100537.

Sun Q, Sun Y, Walker MA, Labavitch JM. 2013. Vascular occlusions in grapevines with Pierce's disease make disease symptom development worse. *Plant Physiology* **161**: 1529–1541. DOI: 10.1104/pp.112.208157.

Tyree MT, Zimmermann MH. 2002. Conducting units: Tracheids and vessels. In: Tyree MT, Zimmermann MH, eds. *Xylem Structure and the Ascent of Sap*. Berlin, Heidelberg: Springer Berlin Heidelberg, 1–25. DOI: 10.1007/978-3-662-04931-0.

Urban J, Dvořák M. 2014. Sap flow-based quantitative indication of progression of Dutch elm disease after inoculation with *Ophiostoma novo-ulmi*. *Trees* **28**: 1599–1605. DOI:

10.1007/s00468-014-1068-0.

Van de Wal BAE, Leroux O, Steppe K. 2018. Post-veraison irreversible stem shrinkage in grapevine (*Vitis vinifera*) is caused by periderm formation. *Tree Physiology* **38**: 745–754.

DOI: 10.1093/treephys/tpx158.

Villalobos-González L, Quintana-Pulido C, Muñoz M, Franck N, Pastenes C. 2018.

Xylem structure and function in three grapevine varieties. *Chilean Journal of Agricultural Research* **78**: 419–428. DOI: 10.4067/S0718-58392018000300419.

Yadeta KA, J. Thomma BPH. 2013. The xylem as battleground for plant hosts and vascular wilt pathogens. *Frontiers in Plant Science* **4**: 97 DOI: 10.3389/fpls.2013.00097.

Accepted Manuscript

TABLES

Table 1. Directly measured or derived quantitative xylem anatomical traits

Acronym	Trait	Unit	Formula	Measurement level
PA	Pith area	μm^2	-	Entire cross section
A_X	Xylem area	μm^2	-	Entire cross section and dorso-ventral area
A_V	Xylem vessel area	μm^2	-	Entire cross section and dorso-ventral area
D	Xylem vessel diameter	μm	$2\sqrt{A/\pi}$	Entire cross section and dorso-ventral area
V_D	Xylem vessel density	nb mm^{-2}	$\frac{\text{nb vessels}}{A_X}$	Entire cross section and dorso-ventral area (calculated either for occluded or non-occluded vessels)
D_H	Hydraulic diameter	μm	$\frac{\sum D^5}{\sum D^4}$	Entire cross section
k_{ts}	Theoretical specific hydraulic conductivity	$\text{kg s}^{-1} \text{m}^{-1} \text{MPa}^{-1}$	$\frac{\pi D^4 \rho}{128 \eta A_X}$	Entire cross section and dorso-ventral area (calculated either for all, occluded or non-occluded vessels)
PLC_{th}	Theoretical percentage loss of conductivity	%	$100 \times \frac{\sum k_{ts \text{ occ.vessels}}}{\sum k_{ts \text{ all vessels}}}$	Entire cross section and dorso-ventral area

FIGURE LEGENDS

Fig. 1. Simplified representation of the normalised distance from the pith (%). The xylem tissue was separated into five portions according to their normalized distance from the pith (0-20; 20-40; 40-60; 60-80 and 80-100 %). The distance of each vessel was measured from the center of the pith and then normalized by measuring the vessel closest to and farthest from the pith in the dorsal and ventral regions. The vessels were then grouped according to the xylem portion. The xylem portions are reported in different colors, while the white point represents the pith center.

Fig. 2. Evolution of the stem standardised maximum daily diameter (MXD in μm) in symptomatic and control stems over one vegetative season in *Vitis vinifera* cv. ‘Sauvignon blanc’ and ‘Cabernet Sauvignon’. Control ‘Sauvignon blanc’ (C2, C3, C4) and ‘Cabernet Sauvignon’ (C1) stems are shown on the left panel and symptomatic ‘Sauvignon blanc’ (S3, S5, S7) and ‘Cabernet Sauvignon’ (S1, S2, S4, S6) stems on the right panel. The points on the curves correspond to the dates of symptom onset.

Fig. 3. Mean growth rate (DGR_w , μm) in symptomatic and control stems over weeks in *Vitis vinifera* cv. ‘Sauvignon blanc’ and ‘Cabernet Sauvignon’. Mean growth rate (DGR_w , μm) comparison between control stems (green line and dots) and symptomatic stems (yellow line and dots) in ‘Sauvignon blanc’ (left panel) and ‘Cabernet Sauvignon’ (right panel). (i) Comparison of the mean growth rate (μm) between control and symptomatic stems of ‘Sauvignon blanc’ for the three typical growth periods of the control plants: the stem growth (before the week 29, “GR”); the shrinkage (between week 30 and 33, “SH”) and the stabilization at the end of the season (between week 34 and 39, “ST”). The vertical bars associated with the data points represent the standard error. The star indicates a significant

DGR_W difference between control and symptomatic ‘Sauvignon blanc’ stems during SH period ($P = 0.01$, Tukey test).

Fig. 4. Percentage of occluded vessels in stems and leaf midribs in *Vitis vinifera* cv. ‘Sauvignon blanc’ and ‘Cabernet Sauvignon’ during esca pathogenesis. A. Percentage of occluded vessels in cross-sections of control and symptomatic stems. No significant differences were found between control and symptomatic stems or between the varieties ($P > 0.05$, ANOVA). B. Percentage of occluded vessels in midrib cross-sections of control (C), asymptomatic (AS, leaves sampled from a symptomatic plant), and symptomatic (S) leaf midribs. The letters represent the differences between leaf symptoms within each cultivar and show that green (C and AS) and symptomatic leaves had a significantly different percentage of occlusions in both varieties ($P < 0.05$, ANOVA).

Fig. 5. Distribution of the vessel density (V_D) in symptomatic and control stems across the normalised distance from the pith (%) in *Vitis vinifera* cv. ‘Sauvignon blanc’ and ‘Cabernet Sauvignon’. A. Occluded vessel density (in nb mm⁻²) B. Non occluded vessel density (in nb mm⁻²). The distance between the pith and the end of the vascular cambium were separated into 20% portions and the xylem vessels distributed between them (as presented in Fig. 1), comparing symptomatic stems and control stems in ‘Sauvignon blanc’ (n = 3 control and n = 5 symptomatic stems, left panel) and in ‘Cabernet Sauvignon’ (n = 3 control, n = 6 symptomatic stems, right panel). (i) Image of a portion of a dorso-ventral xylem section, stained with phloxine infiltration, pink xylem vessels represent functional vessels. Statistical analyses are presented in the Supplementary Table S3.

Fig. 6. Repartition of the vessel diameter in symptomatic and control stems across the normalised distance from the pith in *Vitis vinifera* cv. ‘Sauvignon blanc’ and ‘Cabernet Sauvignon’. ‘Sauvignon blanc’ (n = 3 control and n = 5 symptomatic stems) and ‘Cabernet Sauvignon’ (n = 3 control, n = 6 symptomatic stems) are shown in left and right panels, respectively. Statistical analyses are presented in Supplementary Table S4.

Fig. 7. Theoretical specific hydraulic conductivity and percentage loss of conductivity analysis across the normalised distance from the pith (%) in control and symptomatic stems of *Vitis vinifera* cv. ‘Sauvignon blanc’ and ‘Cabernet Sauvignon’. A. Theoretical specific hydraulic conductivity estimated using all vessels (k_{rs} all vessels). B. Percentage loss of conductivity (%; PLC_{th}). The distance between the pith and the end of the vascular cambium were separated into 20% portions and the xylem vessels distributed between them (as presented in Fig. 1). Each panel shows the comparison between symptomatic and control stems in ‘Sauvignon blanc’ (n = 3 control and n = 5 symptomatic stems, left panel) and in ‘Cabernet Sauvignon’ (n = 3 control, n = 6 symptomatic stems, right panel). Statistical analyses are presented in the Supplementary Table S5-S6. (i) and (ii) PLC_{th} of ‘Sauvignon blanc’ and ‘Cabernet Sauvignon’ whole stem cross sections, respectively ($P > 0.05$ for both cultivars).

Fig. 8. Whole-plant and leaf physiology in control and esca symptomatic *Vitis vinifera* cv. ‘Sauvignon blanc’ and ‘Cabernet Sauvignon’. A. Evolution of the whole plant (canopy) stomatal conductance (G_C , $\text{mmol m}^{-2} \text{s}^{-1}$) according with the beginning of esca symptom expression in weeks (0 correspond to the first apparition of leaf symptoms). B. Leaf-stomatal conductance (g_s , $\text{mmol m}^{-2} \text{s}^{-1}$) measured with a porometer. C. Net CO_2 leaf assimilation (A , $\mu\text{mol m}^{-2} \text{s}^{-1}$) measured with a gas analyser. Panels A and B present three

types of leaves: “C”, leaves from control plants (asymptomatic between June and October 2021); “AS”, asymptomatic leaves from symptomatic plants (both before and after symptom appearance), and “S”, symptomatic leaves (presenting tiger-stripe symptoms). Sample sizes for stomatal conductance (B) were: ‘Sauvignon blanc’, n = 37 “C”, n = 32 “S”, n = 12 “AS”; and ‘Cabernet Sauvignon’, n = 32 “C”, n = 47 “S”, n = 24 “AS” leaves. Sample sizes for CO₂ Assimilation were: ‘Sauvignon blanc’, n = 36 “C”, n = 19 “S”, n = 25 “AS”; and ‘Cabernet Sauvignon’, n = 26 “C”, n = 17 “S”, n = 38 “AS” leaves. Letters indicate statistical significance ($P < 0.05$), for more information see the Supplementary Table S7.

Accepted Manuscript

Figure 1

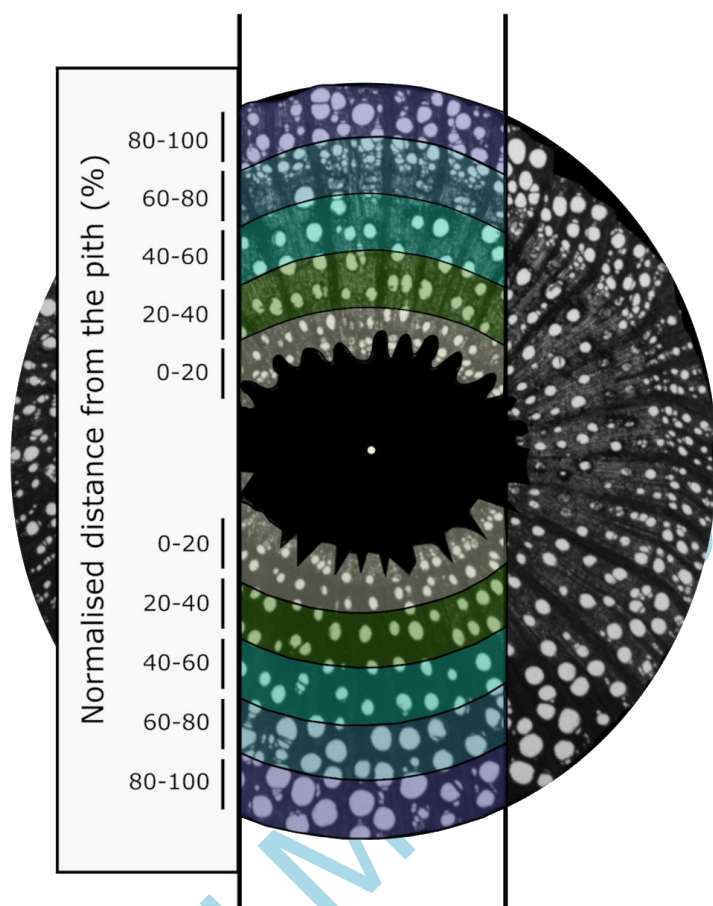


Figure 2

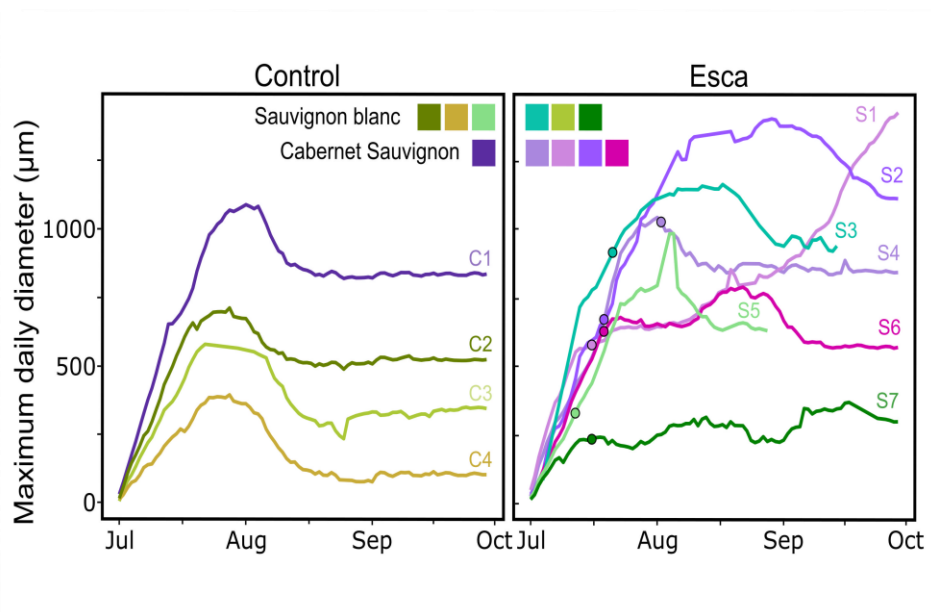
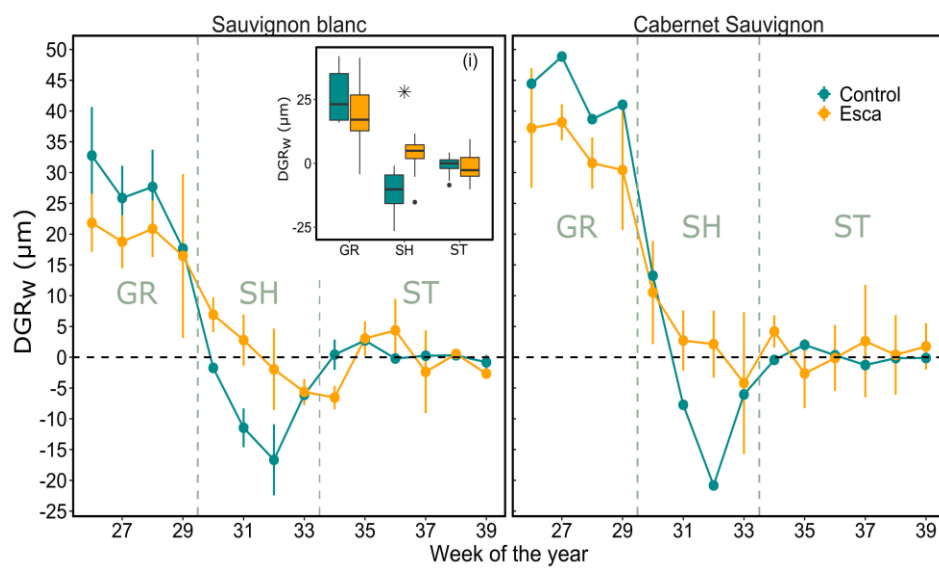
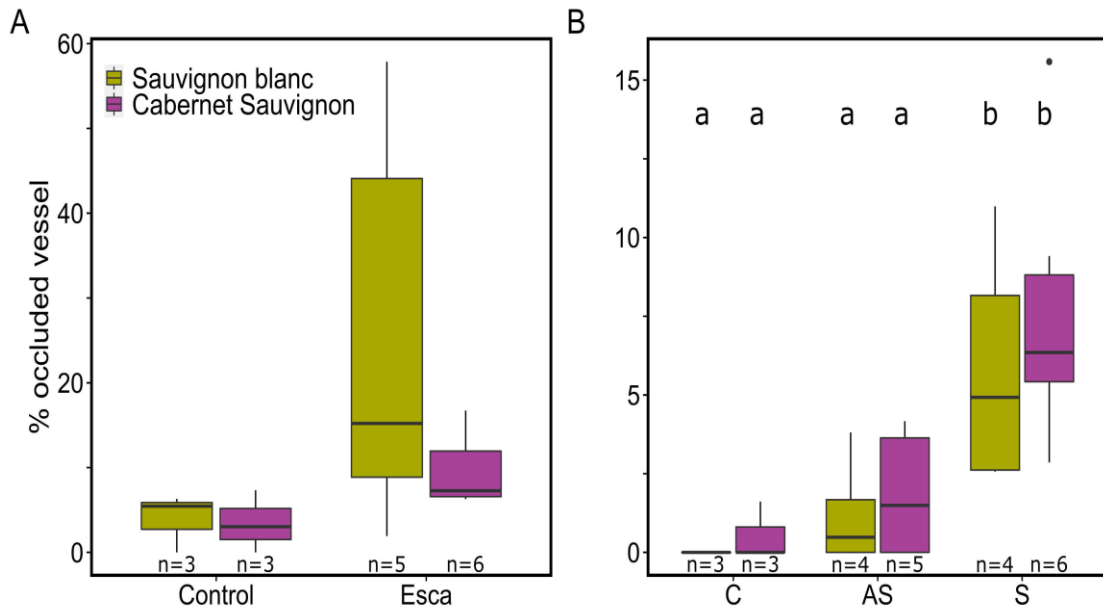


Figure 3



Accepted Manuscript

Figure 4



Accepted Manuscript

Figure 5

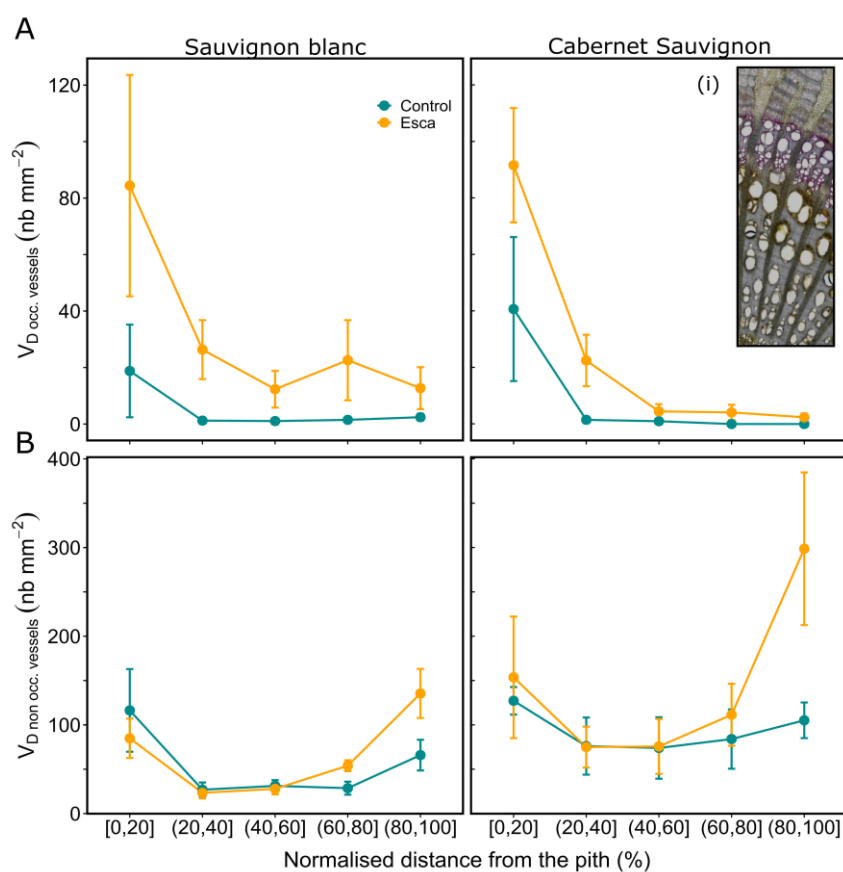
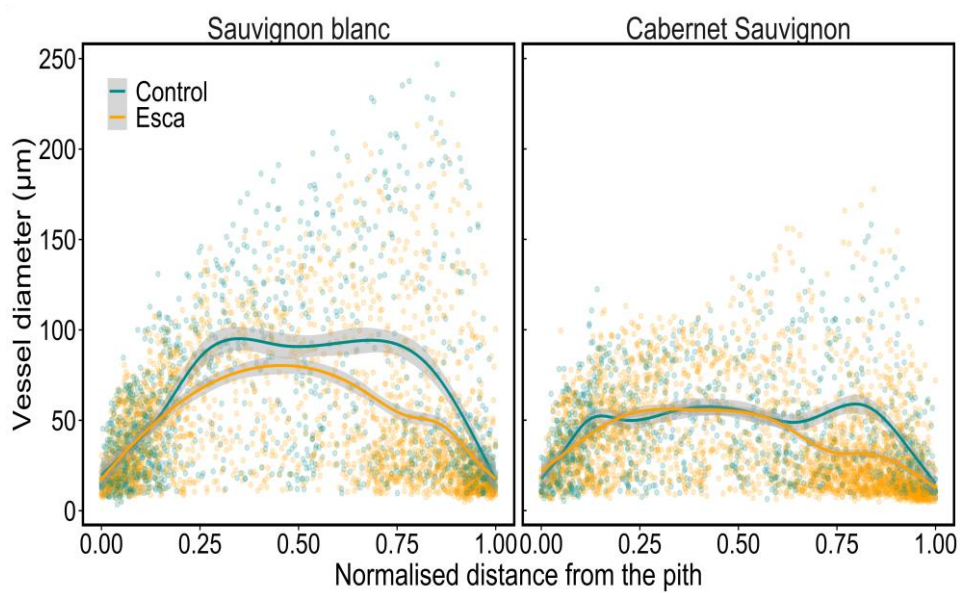


Figure 6



Accepted Manuscript

Figure 7

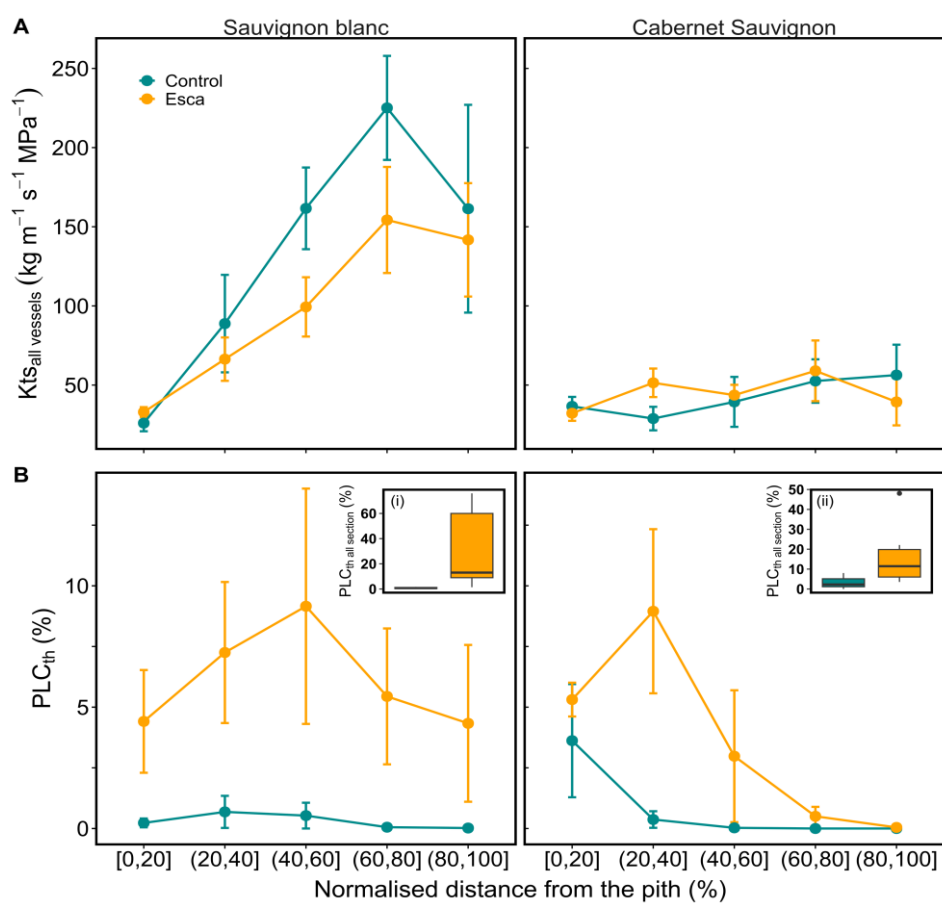
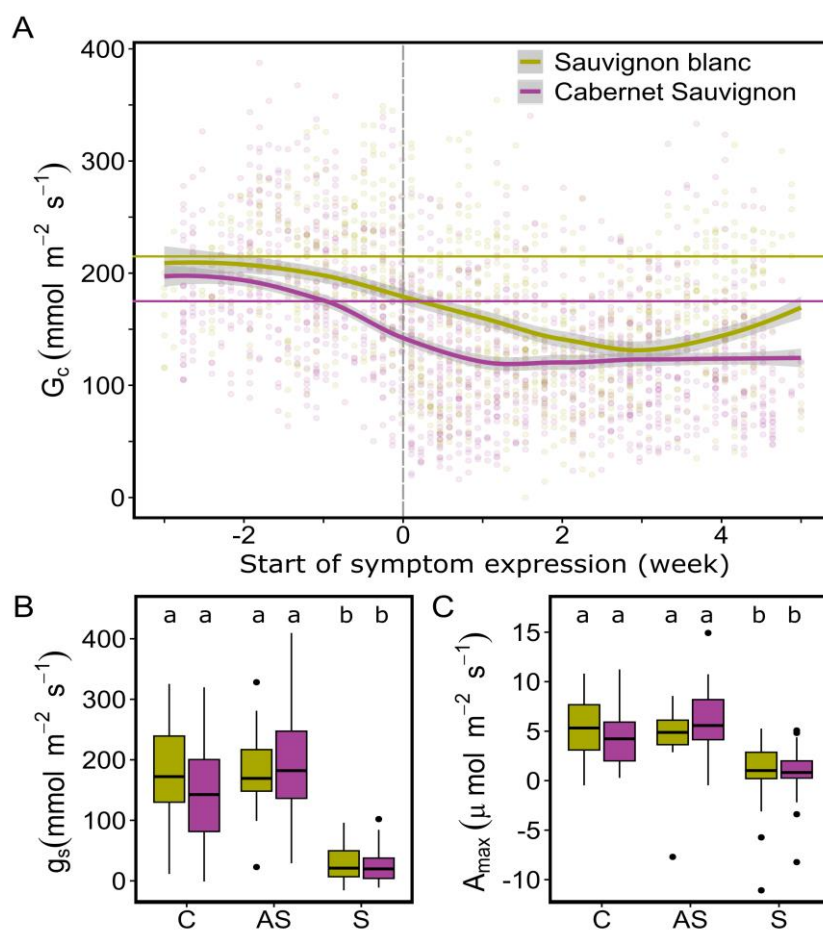


Figure 8



Accepted